

RESEARCH

Open Access



# Prediction of Self-Healing Potential of Cementitious Materials Incorporating Crystalline Admixture by Isothermal Calorimetry

Byoungsun Park<sup>1</sup> and Young Cheol Choi<sup>2\*</sup>

## Abstract

Crack formation is an inherent property of concrete structures; however, these materials also have the ability to heal cracks autogenously. External water penetrates the inside of concrete through the cracks, and unreacted cement particles present on the crack surface are rehydrated. Cracks are healed by hydration products owing to further hydration. Ground-granulated blast-furnace slag (GGBFS) and fly ash (FA) have slower reactions with water than cement. Because of this late reactivity, there is a high possibility of being present in an unreacted state inside the matrix. This study investigated the self-healing potential of supplementary cementitious materials (SCMs) such as GGBFS, FA, and calcium sulfur aluminate (CSA) expansion agents. For this purpose, isothermal calorimetry and water flow tests were performed. Experimental results showed that the self-healing potential of GGBFS and CSA expansion agent was higher than that of OPC and FA is decreased.

**Keywords:** self-healing potential, isothermal calorimetry, further hydration, water flow test, cementitious materials

## 1 Introduction

Cracks in concrete structures are inevitable owing to external loads and time-dependent effects. Cracks make it easier for harmful ions to penetrate into concrete. This reduces the durability of concrete structures. The durability of concrete structures is a key factor that affects the service life and maintenance costs of the structures. Various studies on improving concrete durability performance have been performed. In particular, there has been a growing interest in self-healing concrete that heals cracks naturally (Wua et al. 2012; Jacobsen and Sellevold 1995; Jacobsen et al. 1996; Hearn 1998; Ahn and Kishi 2010).

Generally, concrete has a property that can heal cracks autogenously. The autogenous healing is mainly caused by the precipitation of Calcite, which is formed by the

reaction of  $\text{CO}_3^{2-}$  in the water introduced into the crack and  $\text{Ca}^{2+}$  ions dissolved in the paste, and further hydration reaction in the crack (Edvardsen 1999; Sisomphon et al. 2012). The self-healing properties vary depending on the type of binder and the degree of hydration according to time, and especially with the amount of unreacted cement clinker in the concrete matrix (Huang et al. 2013; Hilloulin et al. 2016). As the cement grains become larger, the cement grains are not fully hydrated and are more likely to remain unreacted. Recently, the early strength of cement was considered to be important. This results in finer cement grains than before. This results in reducing the autogenous healing performance (Tittelboom et al. 2012).

The mechanism of further hydration of unreacted cement grains on a cracked surface is different from that of early cement paste. The water-cement ratio in the crack surface is considerably larger than the initial water-cement ratio because sufficient water is supplied to the crack from the outside. Furthermore, the space in which the hydration product is formed is much larger. This affects the nucleation and growth process of the

\*Correspondence: zerofo@gachon.ac.kr

<sup>2</sup> Department of Civil and Environmental Engineering, Gachon University, 1342 Seongnamdaero, Sujeong-gu, Seongnam-si, Gyeonggi-do 13120, Republic of Korea

Full list of author information is available at the end of the article  
Journal information: ISSN 1976-0485 / eISSN 2234-1315

hydration product and induces a rapid hydration reaction (Hewlett 2004). When the unreacted cement grains on the crack surface come into contact with water, further hydration begins. The  $\text{Ca}^{2+}$  and  $\text{OH}^-$  ions dissolved in unreacted cement begin to diffuse into the crack plane, followed by the diffusion of silicate. Therefore, the concentration of ions increases near the crack plane. When the ion concentration reaches the supersaturation criterion, a new product precipitates around the crack. Unreacted cement grains are present in the paste matrix as well as on the crack surface. The ions dissolved in the unreacted cement present in the paste matrix diffuse to the crack plane at a relatively slow rate. Unreacted cement grains exist not only in the crack plane but also in the paste, and the cement grains in the paste are diffused to the crack surface at a relatively slow speed.

Abdel-Jawad et al. and Granger et al. proved that the autogenous healing property is promoted when the amount of unreacted cement grain increases (Abdel-Jawad and Dehn 2005; Granger et al. 2007). Increasing the amount of unit cement in concrete production can increase the manufacturing cost, the risk of cracking owing to autogenous shrinkage, and the hydration heat (Shen et al. 2018; Hu et al. 2017; Castellano et al. 2016). Many researchers have conducted studies on improving the self-healing performance of concrete by adding mineral admixtures (Hu et al. 2017; Jaroenratanapirom and Sahamitmongkol 2011; Sherir et al. 2016; Termkhajornkit et al. 2009; Darquennes et al. 2016; Huang et al. 2014; Qiu et al. 2016; Salama et al. 2017; Kim and Kang 2017). Ground-granulated blast-furnace slag (GGBFS) and fly ash (FA) have slower reactions with water than cement. This slow reactivity increases the amount of unreacted material and improves the autogenous healing performance. However, GGBFS and FA consume  $\text{Ca}(\text{OH})_2$  supplied by the cement during hydration, which can reduce the amount of  $\text{CaCO}_3$  precipitation (Hu et al. 2017).

Some researchers reported on the cracking self-healing performance of cement composites with the incorporation of GGBFS and FA. Jaroenratanapirom et al. conducted a crack-closing test to evaluate the self-healing performance of FA, silica fume, and crystalline admixture. The test results showed that silica fume was most effective if the crack width was over 0.25 mm. In the case of FA, the self-healing performance decreased when the cracking occurred after 28 days of age (Jaroenratanapirom and Sahamitmongkol 2011). Sherir et al. investigated the mechanical performance recovery based on the self-healing of engineered cementitious materials (ECC) with FA and MgO admixture (Sherir et al. 2016). They examined the performance based on the amount of FA and MgO admixture, which showed that an admixture of FA at 55% and MgO at 5% was most

effective. Termkhajornkit et al. studied the self-healing performance of cementitious materials with FA (Termkhajornkit et al. 2009). They compared the amount of penetrated chloride ions before and after self-healing. The test results showed that the self-healing performance was improved by increasing the fly ash replacement ratio. It was reported that the addition of fly ash increases the pozzolanic reaction. A test showed that an increase in the FA replacement resulted in an improved self-healing performance; the researchers attributed this to the pozzolanic reaction with FA. Sahmaran et al. evaluated the self-healing performance of engineered cementitious composites (ECCs) according to CaO content of fly ash. From the test results, it was confirmed that the self-healing performance was increased when CaO content was high (Sahmaran et al. 2013).

Darquennes et al. studied the resistance to the chloride ion penetration of GGBFS-blended cement based on self-healing (Darquennes et al. 2016). They confirmed that GGBFS resulted in a significant decrease in the coefficient of chloride ions of the crack specimen by the self-healing process. Huang et al. investigated the effect of GGBFS on self-healing products and filling ratio changes and reported that GGBFS improved the self-healing performance (Huang et al. 2014). Qiu et al. analyzed the effect of GGBFS and crack widths on the self-healing performance of ECC (Qiu et al. 2016). They confirmed that the self-healing performance was highest when the substitution amount of GGBFS was 30%. In addition, a variety of studies to utilize fibers and inorganic binders in combination to improve the self-healing performance have been performed (Snoeck and Belie 2015).

Self-healing performance evaluation methods have not yet been standardized, and various methods have been suggested by researchers (Muhammad et al. 2016; Snoeck et al. 2018; Choi et al. 2017). Common methods used to evaluate the self-healing performance of cementitious materials are the water flow rate and the crack closing test. The water flow test measures the change in the flow rate through the cracks, and quantitatively assesses the degree of self-healing by changing the flow rate over time. The water flow test is strongly influenced by the crack characteristics of the test specimens. In particular, as the roughness of the cracks and the impurities in the cracks vary depending on the shape of the cracks, the experimental results are different even in the same material. The healing products observed in the crack closing test are white, usually calcite that precipitated based on the reaction between  $\text{CO}_3^{2-}$  and  $\text{Ca}^{2+}$  on the surface. Therefore, for this method, it is difficult to evaluate the effect of further hydration. The self-healing performance of mineral admixture such as SCMs and crystalline admixture is mainly due to further hydration. Therefore,

in order to predict the self-healing performance of mineral admixture, it is necessary to measure unreacted mineral admixture existing on the crack surface. Huang et al. has studied the method of quantitatively evaluating the unreacted binder around the cracks using the BSE image, but it takes a long time and there is a disadvantage that the measurement of the unreacted binder differs according to the pre-treatment of the specimen (Huang et al. 2013). Further hydration is proportional to the amount of unreacted binder present in the crack. The potential of unreacted binder can be measured easily by measuring heat by further hydration using isothermal calorimetry. Although further hydration measurements using isothermal calorimetry have been performed by Tittelboom et al., there is still a lack of studies about further hydration using isothermal calorimetry (Tittelboom et al. 2012). Release heat due to further hydration of unreacted materials in pastes according to age can be an important parameter of self-healing performance.

In this study, a water flow test was performed to verify the crack self-healing performance according to various mineral admixtures such as GGBFS and FA as well as ordinary Portland cement (OPC). In addition, the self-healing potential by further hydration of unreacted mineral admixtures in the paste was analyzed, and a scanning electron microscopy with energy dispersive spectroscopy (SEM-EDS) analysis of self-healing products was performed.

## 2 Experiment

### 2.1 Materials

In this study, supplementary cementitious materials (SCMs) such as GGBFS and FA were used as binders in addition to OPC. FA and GGBFS used in this study were sourced from Namdong power plant and steel manufacturing company POSCO in Korea. Furthermore, we used calcium sulfoaluminate admixture (CSA) and crystalline admixture (CA) as the expansion material and crystalline agent, respectively. The chemical compositions and physical properties of the binder materials are provided in Table 1.

Figure 1 shows the X-ray diffraction (XRD) patterns of the binder materials. The OPC was composed of  $C_3S$ ,  $C_2S$ ,  $C_3A$ ,  $C_4AF$ , gypsum, and quartz. According to the Rietveld method analysis (Table 2), the mineralogical composition is 62 wt%, 16.1 wt%, 2.5 wt%, 12.1 wt%, 0.2 wt%, and 2.6 wt% of OPC, respectively. GGBFS includes only anhydrite (2.9 wt%) and quartz (2.1 wt%) in its crystalline phase. FA is composed of 74.4 wt% of glass phase, 11.3 wt% of quartz, and 13.9 wt% of mullite. CSA has gypsum, CaO, CSA, mayenite, and  $C_3S$ , among others. The CSA expansion agent contains 48.6 wt% of gypsum,

**Table 1 Chemical compositions and physical properties of raw materials.**

	Chemical compositions (%)			
	OPC	CSA	GGBFS	FA
SiO <sub>2</sub>	16.91	3.87	32.54	53.73
Al <sub>2</sub> O <sub>3</sub>	3.95	9.63	13.34	20.05
Fe <sub>2</sub> O <sub>3</sub>	3.12	0.78	0.45	5.57
CaO	57.85	48.89	42.28	3.36
MgO	1.66	0.65	2.52	0.91
K <sub>2</sub> O	1.24	0.20	0.56	1.45
Na <sub>2</sub> O	0.23	–	0.21	0.96
TiO <sub>2</sub>	0.25	0.44	0.57	0.98
MnO	0.20	–	0.24	0.07
P <sub>2</sub> O <sub>5</sub>	0.46	0.42	–	0.26
SO <sub>3</sub>	1.71	16.41	2.09	0.45
SrO	0.06	0.06	0.06	0.10
Physical property				
Density (kg/m <sup>3</sup> )	319	278	287	210
Surface area (m <sup>2</sup> /kg)	3880	4630	4280	3480

28.0 wt% of CSA, and 16.6 wt% of Ca(OH)<sub>2</sub>, as well as 1.7 wt% of mayenite, which is a component of C<sub>12</sub>A<sub>7</sub>.

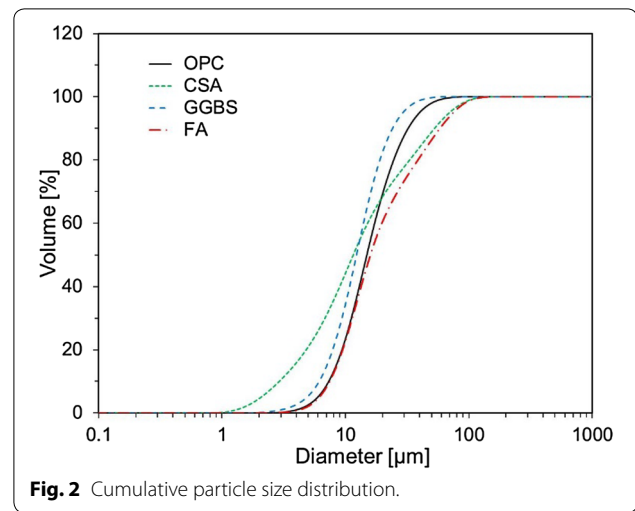
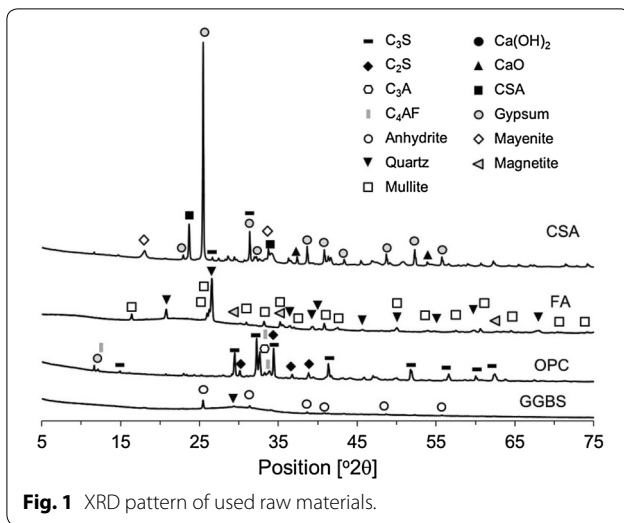
Figure 2 shows the particle size distribution of the binder materials. The average particle sizes of OPC, GGBFS, FA, and CSA are 19.1, 15.0, 26.9, and 21.9 μm, respectively. OPC ranged from 2 to 40 μm, and CSA had a wider range of particle sizes (from 0.9 to 100 μm) than OPC. FA had a particle size distribution that was similar to that of OPC at lower particle sizes; however, its maximum size was 100 μm, which was higher than that of OPC. GGBFS had particle sizes ranging from 1 to 20 μm, which was smaller than that of OPC.

Table 3 lists the proportions of the binders in paste mixtures. The main variables are the type and replacement ratio of SCMs and the type and amount of CA. The addition of GGBFS (60 wt%), FA (35 wt%, 50 wt%) and CSA (10 wt%) with various CA such as CaSO<sub>4</sub>, Na<sub>2</sub>SO<sub>4</sub>, and MgCO<sub>3</sub>, and Xypex, a commercial self-healing product, was investigated to evaluate the self-healing potential and performance. All binders in powder form were pre-mixed for 30 s by using a mixer. The water-binder (W/B) ratio of the isothermal calorimetry was set to 0.35, and that of the water flow test was to 0.35.

### 2.2 Test Methods

#### 2.2.1 Heat of Hydration

In this study, isothermal calorimetry was used to evaluate the potential for self-healing owing to further hydration of unreacted binder in the crack. The isothermal calorimetry used in this test was TAM-AIR, which



**Table 2** Mineralogical phase composition of raw materials.

	OPC	GGBFS	FA	CSA
Glass phase	–	95.0	74.4	–
C <sub>3</sub> S	62.0	–	–	3.2
C <sub>2</sub> S	16.1	–	–	–
C <sub>3</sub> A	2.5	–	–	–
C <sub>4</sub> AF	12.1	–	–	–
Gypsum	2.6	–	–	48.6
Anhydrite	–	2.9	–	–
Quartz	0.2	2.1	11.3	–
Mullite	–	–	13.9	–
Magnetite	–	–	0.4	–
CaO	–	–	–	2.0
Ca(OH) <sub>2</sub>	–	–	–	16.6
Mayenite (C <sub>12</sub> A <sub>7</sub> )	–	–	–	1.7
CSA	–	–	–	28.0

can measure the hydration heat in eight channels at the same time, and up to 20 g of paste specimens per sample can be tested for hydration heat. To evaluate the self-healing potential based on the further hydration of inorganic binders, we measured the hydration heat at ages of 0, 7, and 91 days. The reference hydration heat was measured in the case of 0 days. In this study, a total of 100 g of binders based on the mixture proportions listed in Table 3 were mixed with 35 g of tap water. Afterward, ampules were filled with approximately 5 g of each variable. After measuring their weights, the ampules were placed into a calorimeter in order to measure the hydration heat.

Paste specimens with the same mixture proportion as listed in Table 3 and a size of 10 mm × 10 mm × 10 mm were fabricated for evaluating the self-healing potential after 7 days and 91 days. The specimens were cured for 1 day in a humid chamber (RH > 95%, 20 ± 3 °C). After demolding, the specimens were further cured in a water container at 20 ± 3 °C before the self-healing potential test was conducted. The water-cured specimen for the aimed aging periods (7 and 91 days, respectively) was dried for 6 h in a chamber at 40 °C before being crushed into powdered specimens. The powdered specimens were sieved with a sieve of 200 μm in size. After mixing 10 g of the prepared powder specimen and 4 g of tap water, approximately 5 g of the paste was placed in the ample for the test. The temperature change was measured every 1 min, and the amount of hydration heat was measured for 2 days (48 h).

**2.2.2 Water Flow Test**

A water flow test was performed to evaluate the self-healing performance. In this test, three disk specimens with a mixing ratio shown in Table 3 and a size of φ50 × 25 mm were fabricated. After mixing, the specimens were cured for 24 h in a humid chamber (RH > 95%, 20 ± 3 °C). After demolding, the specimens were cured in a water container at 20 ± 3 °C for 6 days. A crack in the specimen was induced by a splitting tensile strength test. Broken-off particles in the crack of the specimen were cleared. A copper wire with a diameter of about 0.2 mm was placed into the crack so that the crack width was consistent after the specimen was completely separated into two pieces. Then, both sides of the specimen were fixed with epoxy. Figure 3 shows the prepared specimen for the water flow test. To prevent any changes in the crack width during the test, the specimen was fastened with a rubber ring,

**Table 3 Mixture proportions of binders.**

Variables	Binder (g)							
	OPC	GGBFS	FA	CSA	CaSO <sub>4</sub>	Na <sub>2</sub> SO <sub>4</sub>	MgCO <sub>3</sub>	Xypex <sup>a</sup>
Plain	100.0	–	–	–	–	–	–	–
F35	65.0	–	35.0	–	–	–	–	–
F50	50.0	–	50.0	–	–	–	–	–
G60A5	35.0	60.0	–	–	5.0	–	–	–
G60N5	35.0	60.0	–	–	–	5.0	–	–
C10X	88.5	–	–	10.0	–	–	–	1.5
C10MX	86.0	–	–	10.0	–	–	2.5	1.5

<sup>a</sup> Xypex Admix C-1000NF, Xypex Chemical Corporation, Canada.

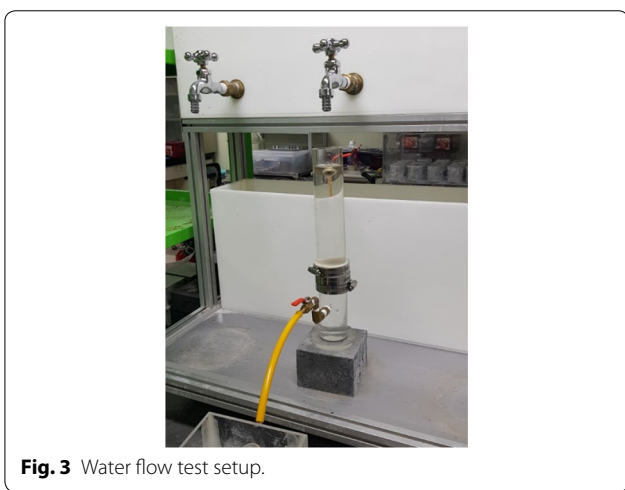


**Fig. 3** Water flow test setup.

and a steel clamp was used to tighten the specimen. The crack width of the specimen was measured. The water flow test was performed with the height of the hydrostatic head at 160 mm (including the length of the specimen), and the test used tap water at  $20 \pm 3$  °C. The water flow test was performed for 56 days. The water flow was measured for 1 min during each measurement.

Table 4 lists the results of the crack width measurements. The crack widths were measured at 1/4, 1/2, and 3/4 positions in the cross-section direction of the specimen, and the average and standard deviation of the measured results were calculated. According to Table 4, the average crack width ranged from 0.210 to 0.301 mm.

### 3 Experimental Results and Discussion

#### 3.1 Self-Healing Potential

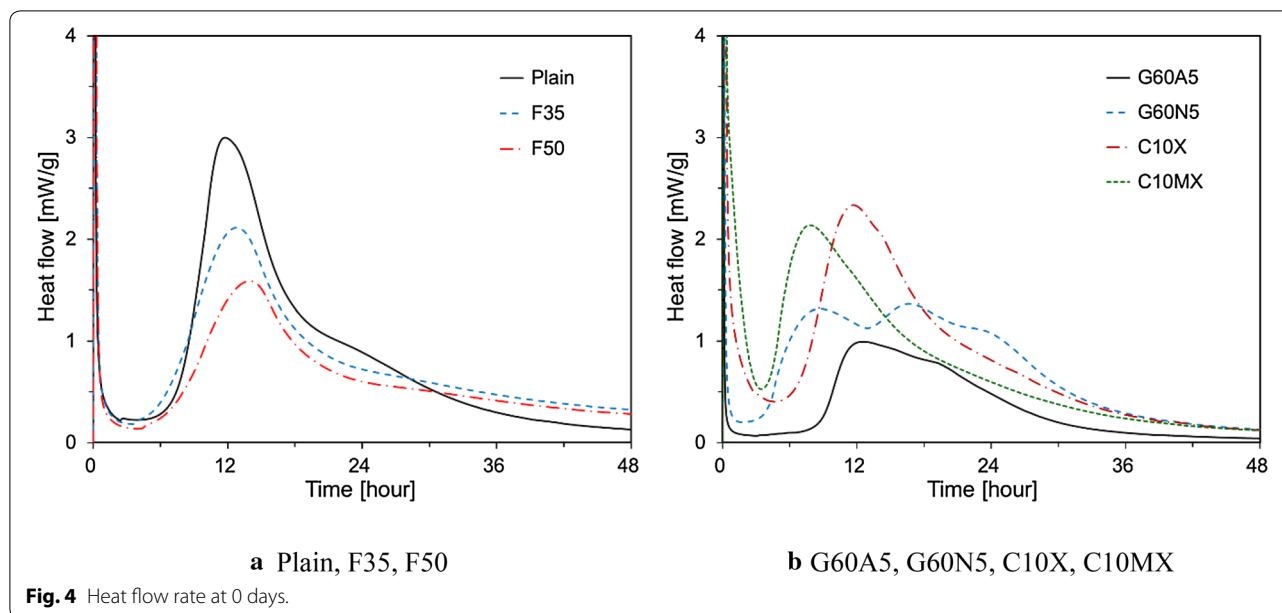
Figure 4a, b show the heat flow rate at 0 days. Figure 4a shows the results of Plain, F35, and F50, while Fig. 4b shows G60A5, G60N5, C10X, and C10MX. Plain in Fig. 4a showed a second peak at about 12 h. An increase in the amount of FA constitution resulted in a decrease

**Table 4 Measured surface crack widths of specimens.**

Labels	Initial crack width (mm)	
	Mean	S.D.
Plain	0.241	0.039
F35	0.301	0.016
F50	0.215	0.033
G60A5	0.273	0.016
G60N5	0.253	0.035
C10X	0.210	0.024
C10MX	0.295	0.016

in the size of the second peak. In addition, the induction period and the occurrence time of the second peak also increased slightly. F35 and F50 showed a similar dormant period as that of Plain. FA did not significantly influence the hydration of OPC, and the second peak decreased in proportion to the replacement ratio.

In the case of GGBFS (G60A5, G60N5), the replacement ratio was 60%, the initial heat flow was lower than that of the others, and different patterns of heat flow appeared based on the crystalline admixture type. G60A5 with anhydrite showed the longest induction period, and the second peak was observed to be low. However, G60N5 with Na<sub>2</sub>SO<sub>4</sub> resulted in a short induction period and a high second peak compared to G60A5. Na<sup>2+</sup> is more soluble and more highly reactive than Ca<sup>2+</sup>. For this reason, the specimen with Na<sup>2+</sup> admixture showed a shorter induction period than the specimen with anhydrite (Mota et al. 2018). In addition, as shown in Fig. 4b, C60N5 showed a “shoulder” in the specific heat flow during the deceleration period after the second peak. This was considered to be related to the consumption of calcium sulfate owing to ettringite or aluminum iron mono (AFm) resulting from the second aluminate reaction (Bouzoubaa et al. 1999; Richardson et al. 1989; Lerch



1946; Gallucci et al. 2010; Hesse et al. 2011; Le Saoût and Haha 2011).

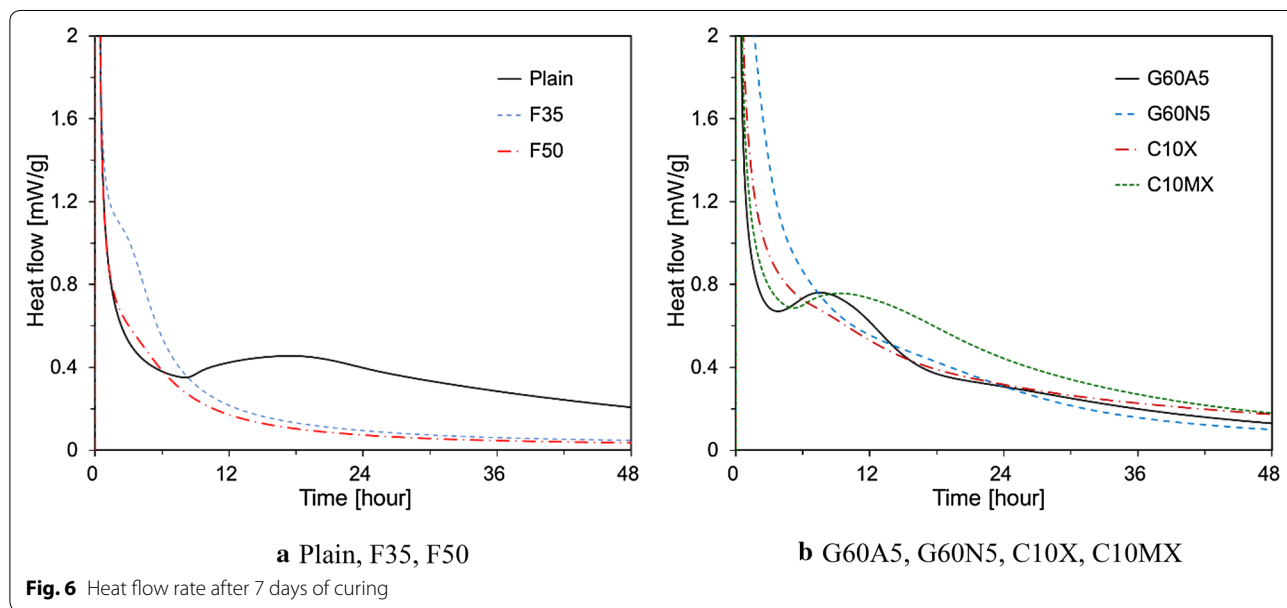
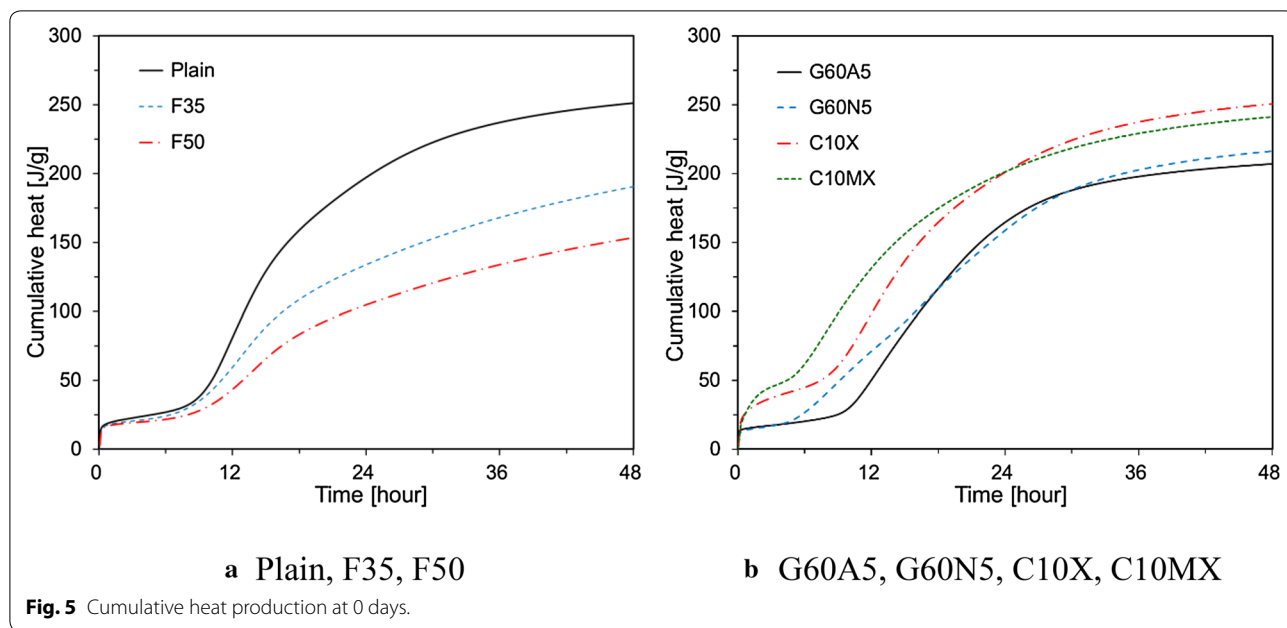
In the case of C10X and C10MX with CSA, the second peak, which was related to the hydration of  $C_3A$ , decreased. This result is similar to that of Nocun-Wczelik et al. (Nocun-Wczelik et al. 2012). Plain showed a small shoulder at about 24 h after the second peak. C10X and C10MX with a 10% substitution of CSA showed a very short induction period. In particular, C10MX was shown to have approximately 7 h of a second peak. It was considered that the higher reactivity of CSA and the influence of  $MgCO_3$  result in shortening induction period compared with the others. The flow rate within 48 h showed that Plain had a lower heat flow than the other compositions; this confirms that the hydration of Plain decreases after 48 h.

Figure 5 shows the cumulative heat release of the fresh paste. As expected from the results of the heat flow rate, the cumulative heat of Plain, C10X, and C10MX was shown to be high; however, that of FA decreased with an increasing substitution rate. As for the specimen with GGBFS, the cumulative heat after 48 h was similar regardless of the type of crystalline admixture. The induction period of G60N5 was shorter than that of G60A5, and the slope started to increase after about 6 h. C10X and C10MX containing CSA had a brief induction period. Thus, from the earliest period, the cumulative heat production continued to increase. In particular, C10MX showed the fastest reaction speed. However, C10X showed the highest cumulative heat production for 48 h, through which it was determined that the amount of

the reaction before 24 h was high; however, it decreased after 24 h.

Figure 6 shows the heat flow rate by the further hydration of unreacted binders in the paste after 7 days of curing. In the case of Plain, it was confirmed that there was a second peak owing to further hydration of the unreacted cement in 7 days cured specimen. This was owing to the existence of sufficient unreacted cement whose induction period appeared even after 7 days. This was similar for G60A5 and C10MX. On the other hand, no induction period appeared for F35, F50, G60N5 and C10X. According to Odler, the induction period does not exist during the further hydration of unreacted cement particles owing to the existing hydration products in the crack plane. This is because the existing hydration products act as seeds of new hydration products and promote the hydration of the cement particles (Odler and Dorr 1979).

Given that a small number of unreacted cement particles existed on the cracked surface, the water-cement ratio that can react in the cracked areas was shown to be higher than that of the initial cement paste. According to the literature, the reaction of cement with a significantly high water-cement ratio can become increasingly fast (Huang et al. 2013). As a result, the amount of hydration products formed in the cracks increases considerably at the initial stage after crack occurrence. The new hydration products formed on the cracked surface, particularly on the surface of the unreacted cement particle in crack plane, form a new layer. This makes it difficult for the dissolved ions inside the

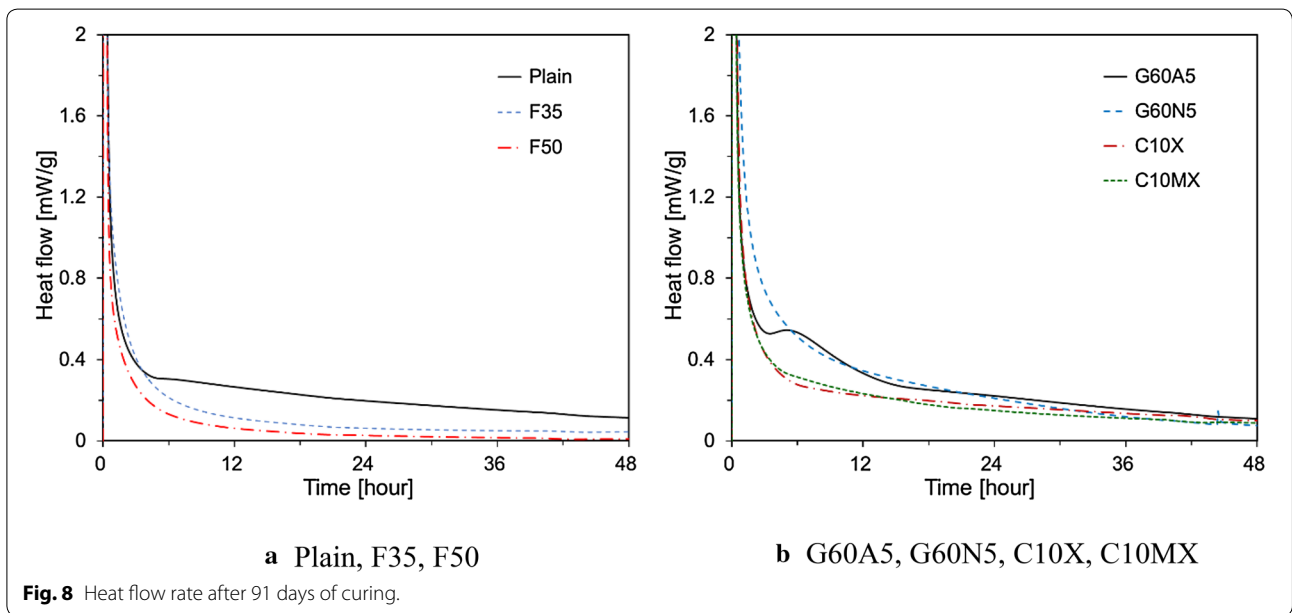
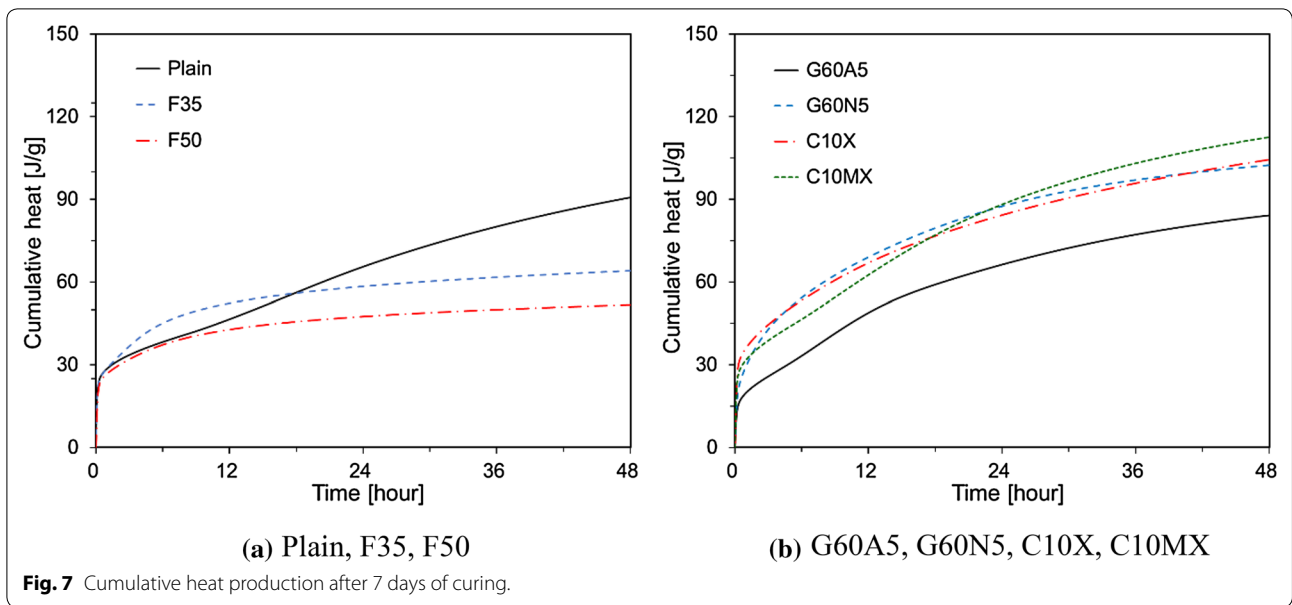


matrix to migrate to the crack surface, thereby slowing the production of additional hydrates.

Figure 7 shows the cumulative heat by the further hydration of unreacted binders in the paste after 7 days of curing. The cumulative heat of Plain for 48 h was approximately 90 J/g, and the FA reduced the cumulative heat production.

The cumulative heat of Plain was lower than that of FA until 18 h because the initial reaction rate decreased owing to the induction period in the further hydration

process. The cumulative heat of G60N5 with  $\text{Na}_2\text{SO}_4$  was increased compared to Plain; however, that of G60A5 with anhydrite showed a slightly lower result than Plain. This is a different result from Tittelboom et al. who showed that GGBFS increased the cumulative heat (Tittelboom et al. 2012). Both C10X and C10MX increased the cumulative heat compared to Plain. While it was expected that the amount of unreacted materials would decrease considerably because the reaction speed of CSA was faster than OPC, a large

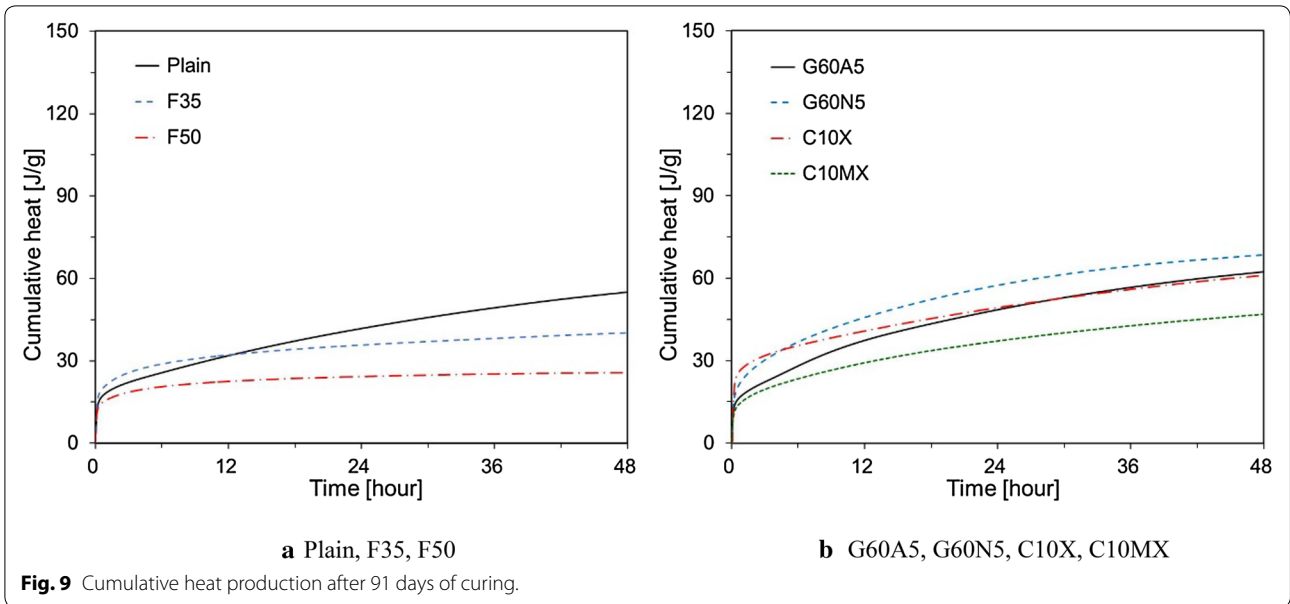


amount of CSA remained as unreacted material after 7 days of curing. When FA was used, the cumulative heat converged at 48 h in contrast to the other variables. This is because it is believed that further hydration was almost completed within 48 h, while the cumulative heat of the other variables continued to increase.

Figure 8 shows the heat flow rate by the further hydration of unreacted binders in the paste after 91 days of curing. As shown in Fig. 8, F35 and F50 converged almost to a zero heat flow rate after 24 h. The heat flow rate at 91 days was considerably lower than that at 7 days for

all variables and did not show an induction period. As a result, it was confirmed that the amount of unreacted binders that can be rehydrated in the case at 91 days of age was smaller than that at 7 days of age.

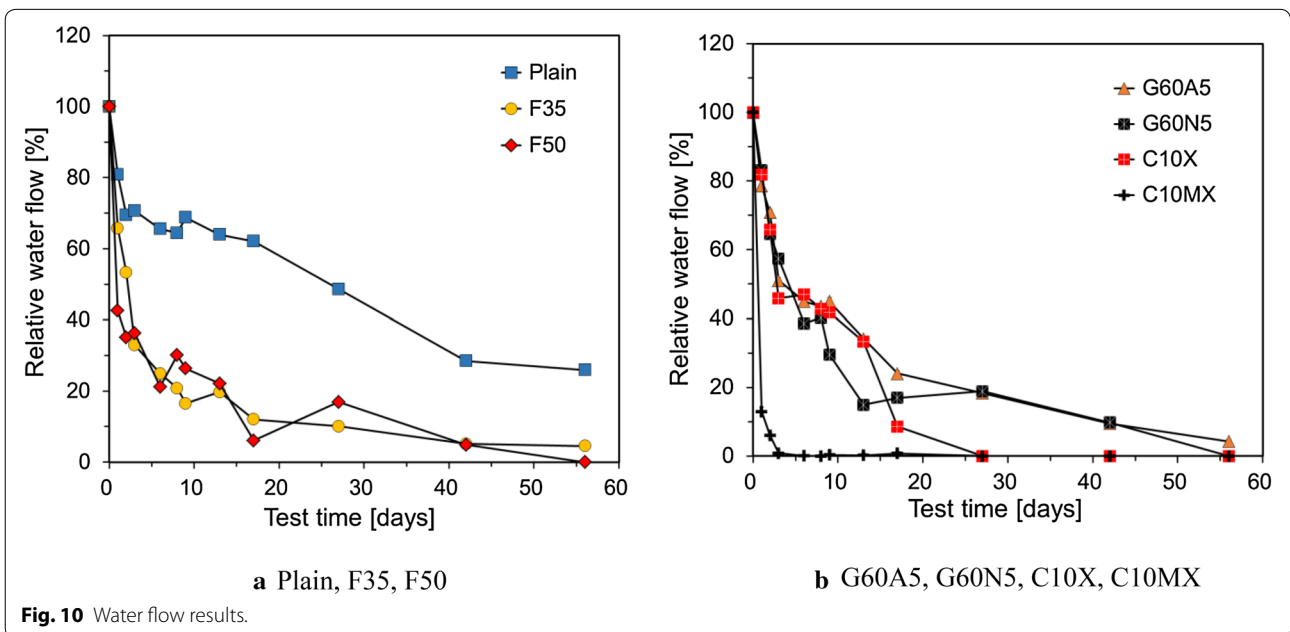
Figure 9 shows the cumulative heat by the further hydration of unreacted binders in the paste after 91 days of curing. Similar to the results in Fig. 8, the cumulative heat of F35 and F50 barely increased after approximately 24 h. The other variables showed an increasing slope even after 48 h. As a result, it was expected that the cumulative heat of the other variables would increase after 48 h,



similar to the results of 7 days, as shown in Fig. 7. In this study, when the self-healing potential indicated by the calorimetric measurement from further hydration was evaluated, FA reduced the self-healing potential. It was shown that the cumulative heat of G60N5 at 91 days of curing was the highest, which was identical to the results after 7 days of curing. The cumulative heat production of G60A5 and C10X was almost similar to each other; however, that of C10MX decreased from that of Plain.

### 3.2 Water Flow Test Results

Figure 10a shows the results of a water flow test of Plain, F35 and F50. Water flow test was performed using paste specimens at the ages of 7 days. For Plain, the water flow decreased by approximately 30% for the first 3 days, and by approximately 70% at 56 days. Compared to Plain, the water permeability of FA35 and FA50 with FA was improved by self-healing. Both specimens indicated that the water flow decreased by more than 65% within 5 days.



The water flow of F35 and F50 after 56 days was approximately 5% and 0%, respectively. A water flow value close to zero indicates that the crack has completely healed.

The results of these water flow tests showed a tendency different from the self-healing potential analysis results through the hydration heat measurement. In the case of the water flow test, there are various parameters that affect the change of water flow in addition to the self-healing mechanism by the further hydration of unreacted binders. Figure 10b shows the water flow test results of G60A5, G60N5, C10X, and C10MX. It was found that all four variables had improved self-healing performance compared to Plain. In particular, the specimen containing a CSA expansion admixture showed a drastic decrease in the amount of water permeation. In this case, similar to the result from the specimen with FA, the result was contrary to the results of the hydration heat measurement.

A comparison of the cumulative heat based on further hydration after 7 days curing showed that G60A5 had a smaller cumulative heat than Plain; however, the water flow reduction was higher than Plain. For the other variables, the cumulative heat was not much different from that of Plain; however, the water flow test results were considerably different from those of Plain.

The difference between the cumulative heat results by further hydration and the water flow test results is considered to result from three causes. The first is the difference in the shape of the induced cracks for the performance of the water flow test. In this study, the crack width was fixed with a copper wire with a diameter of 0.25 mm inside the cracks in order to induce cracks with identical gaps. However, as shown in Table 4, the crack width was different for each specimen. This is because the cracked surfaces in the crack induction process result in different shapes, and it was impossible to introduce cracks with identical widths.

In addition, the shape of the cracked surfaces differed for each specimen. Owing to the different crack shapes, different water flow results were observed even with the same crack width, which might have resulted in reducing the water flow in the cracks. M. Roig-Flores et al. proposed that a self-healing product is generated in a narrow-cracked region, as shown in Fig. 11, which results in reducing the water flow (Roig-Flores et al. 2015). Therefore, even with identical self-healing potentials, specimens result in different water flow values depending on the shape and crack width. In particular, the crack width of F50 is smaller than that of Plain or F35; hence, its water flow is considered to have a smaller value.

The second explanation results from the difference in the volume of the self-healing products produced by further hydration. The hydration products generated in the

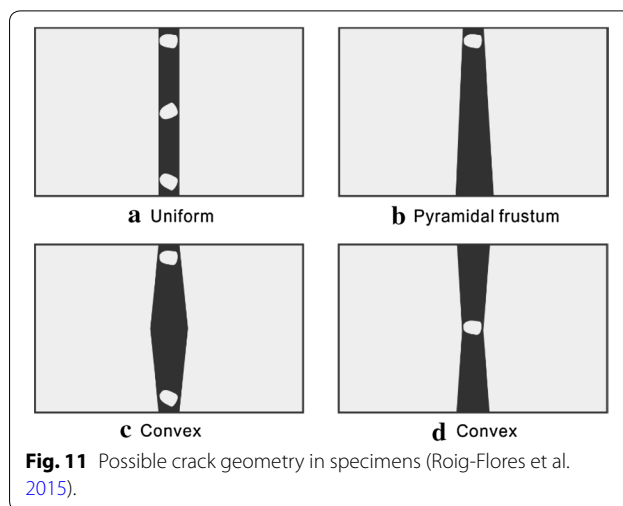
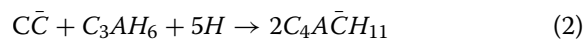
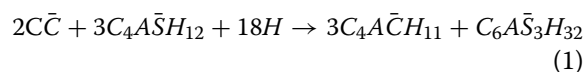


**Fig. 11** Possible crack geometry in specimens (Roig-Flores et al. 2015).

hydration process of inorganic binders have different volumes by type, and if the volume of the hydrates expands, the self-healing performance can be improved even with an identical amount of unreacted binders. When using  $\text{Na}_2\text{SO}_4$  and CSA as crystalline admixtures, ettringite and other expansive hydrates are produced as self-healing products generated in the cracks, and these products improve the self-healing performance. This results in a difference in the water flow test results and the results of the self-healing potential as evaluated by measuring the cumulative heat of unreacted binders (Sisomphon et al. 2012). Equation (1) is a reaction equation that generates calcium carboaluminate hydrate and ettringite by the reaction of calcite and AFm, which is generated by the supply of sulfate. The volume of the precipitate formed through this reaction increases by approximately 23%. (Day 1992). Equation (2) shows the reaction that generates calcium carboaluminate hydrate with the reaction of calcite with hydrogarnet, which is produced by the supply of aluminum. This results in a volume increase of approximately 40% (Ferreiro et al. 2013).



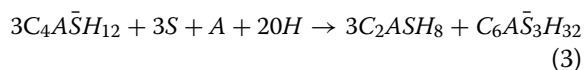
The third reason relates to the mechanism that generates the precipitation of  $\text{CaCO}_3$  as  $\text{Ca}^{2+}$ , which exists in the paste matrix, moves to the cracks, and reacts with  $\text{CO}_3^{2-}$ , which is dissolved in the water permeated to the cracks. This mechanism takes place over a very long period of time because the supply of  $\text{CO}_3^{2-}$  from the penetrated water and the migration of  $\text{Ca}^{2+}$  from the cement matrix to the cracks occur slowly. In order to accurately evaluate the mechanism of self-healing by

calcite precipitation, it is considered necessary to conduct a long-term experiment over 60 days.

The crack self-healing mechanisms by inorganic binders are divided into two categories: the first mechanism is self-healing by further hydration of unreacted binders in the cracks, and the second is the  $\text{CaCO}_3$  precipitation mechanism based on the diffusion of  $\text{Ca}^{2+}$ , which exists in the paste matrix (Roig-Flores et al. 2015). The hydration heat generated in the further hydration process of unreacted binders can be measured by an isothermal calorimetry test, while the self-healing performance based on the  $\text{CaCO}_3$  precipitation from the diffusion and dissolution of  $\text{Ca}^{2+}$  cannot be easily determined. Thus, the result showed a difference compared to the water flow test results.

### 3.3 Scanning Electron Microscopy

To analyze the difference between the hydration heat measurement results and the water flow test results, the self-healing products were analyzed by scanning electron microscopy (SEM). After the water flow test, the self-healing material in the crack of the specimen was carefully scraped with a plastic scraper and dried in a  $40^\circ$  oven to prepare a sample for SEM analysis. Figure 12 shows the SEM analysis results for the self-healing substances. The main product of Plain was  $\text{Ca}(\text{OH})_2$ , and it was confirmed that some  $\text{CaCO}_3$  and C–S–H were produced. In the case of F35, amorphous and  $\text{CaCO}_3$  as well as stratlingite were produced. When fly ash was incorporated, the monosulfate produced by OPC became stratlingite and ettringite, as shown in Eq. (3). (Martin et al. 2017).



Equation (3) is a reaction in which monosulfate is formed by OPC hydration, and the pH is increased. Therefore, when the pH is increased owing to the dissolution of the unreacted material in a small amount of water penetrating into the crack surface as in the water flow test, the reaction in Eq. (3) can occur. However, when the compounding water amount is increased as in the isothermal calorimetry test, the pH may not increase, and the reaction may not occur. For this reason, the cumulative heat production measured by isothermal calorimetry was decreased compared to Plain when mixed with fly ash; however, the self-healing performance measured by water flow tests was increased compared to Plain when mixed with fly ash. Figure 12c, d show SEM observation of the self-healing products of G60N5 and G60A5. In the case of G60A5 and G60N5, it was confirmed that mainly amorphous substance was observed not in the crystal phase hydrate.

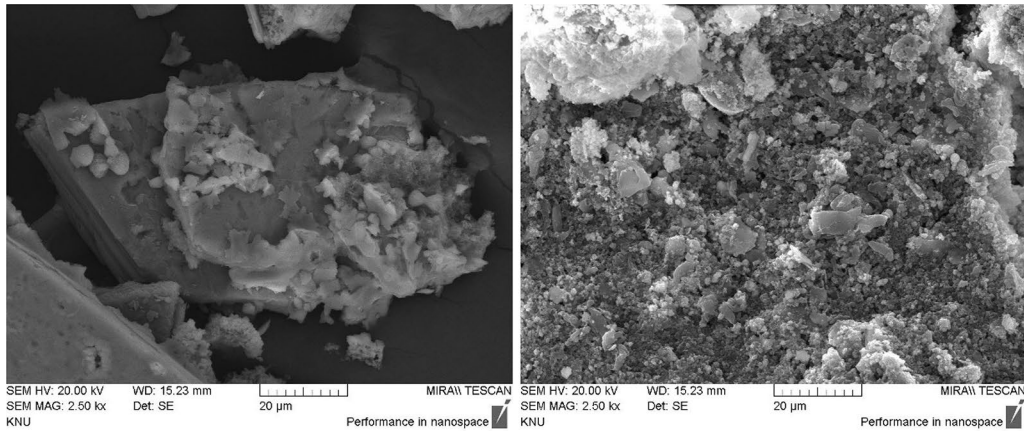
To investigate the self-healing products of G60A5 and G60N5, an SEM–EDS analysis was performed as shown in Fig. 13. As a result, Al ions were observed owing to the incorporation of GGBFS, and it was confirmed that Al-containing hydration products such as OH-hydro-talcite and hydrogarnet ( $\text{C}_3\text{AH}_6$ ) were formed in addition to  $\text{CaCO}_3$  and C–S–H. From the EDS analysis, it was predicted that Point 1 shows Calcite and Point 2 shows hydrogarnet. Hydrogarnet by the incorporation of GGBFS reacted when  $\text{CO}_3^{2-}$  penetrated from the outside and generated  $\text{CaCO}_3$ .

In the case of C10X, ettringite produced by  $\text{SO}_3^{2-}$  and  $\text{Al}^{3-}$  supplied by the CSA expansion agent was seen, and  $\text{CaCO}_3$  production was promoted by  $\text{Ca}^{2+}$ . Ettringite is a needle-shaped hydrate whose volume expands and is believed to effectively fill the cracks. C10MX showed brucite generated by the  $\text{MgCO}_3$  as well as the ettringite generated by the CSA expansion agent. Both hydrates are expansive hydrates and are effective in crack healing. During the water flow test, they helped to quickly reduce the water flow in the initial period of the test.

## 4 Conclusions

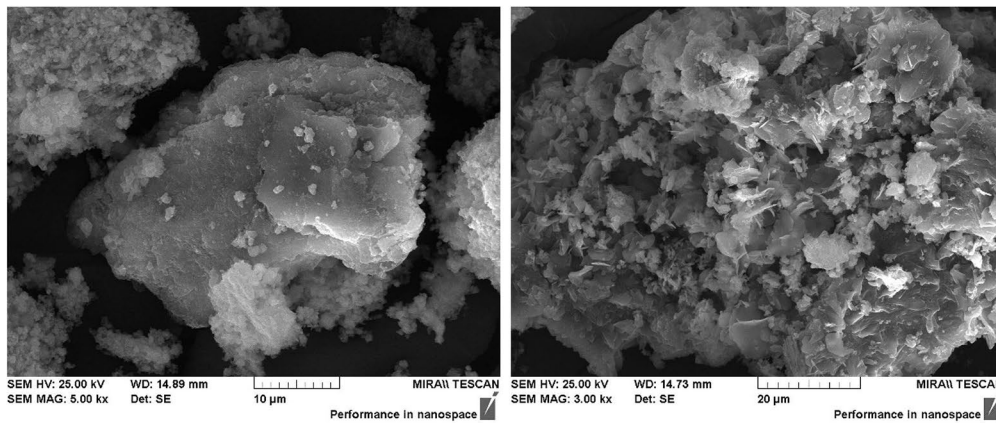
In this study, isothermal calorimetry tests were conducted to investigate self-healing potentials by further hydration of inorganic binders. Cubic specimens of  $10 \text{ mm} \times 10 \text{ mm} \times 10 \text{ mm}$  in size were prepared to measure hydration heat by further hydration of inorganic binders. The samples were crushed and sieved at 7 and 91 days of curing to be used in the test. In the case of FA, the cumulative heat production owing to further hydration was decreased as compared to Plain. For GGBFS, CSA expansion agent, and crystalline admixtures, the cumulative heat production increased. This tendency was shown to be more significant among specimens at 91 days than at 7 days; the hydration heat of specimens at 91 days of curing with GGBFS and CA was the highest. As the amount of FA increased, the cumulative heat production decreased. It was judged that the crushed sample did not reach the pH required for an FA reaction because the unreacted OPC clinker was not sufficient. However, the specimen with GGBFS and CA showed an increase in the unreacted binders inside the paste owing to the relatively slow reactivity of GGBFS, which resulted in an increase in the hydration heat based on further hydration. Owing to the fast hydration speed of CSA, the specimen with the CSA expansion agent did not have sufficient hydration of OPC, which resulted in an increase in unreacted binders compared to Plain.

For a comparative analysis of the hydration heat by isothermal calorimetry, a water flow test was performed. The test results showed that the water flow reduction of Plain was smallest, and as opposed to



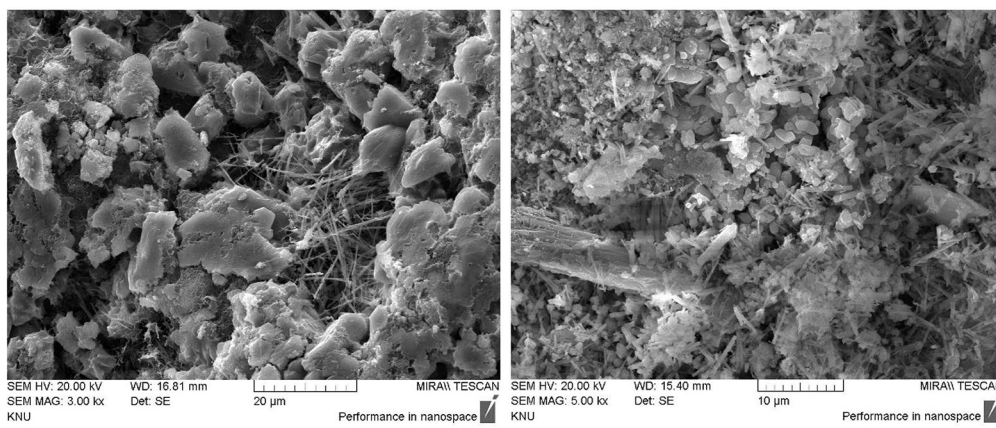
**a** Plain

**b** F35



**c** G60A5

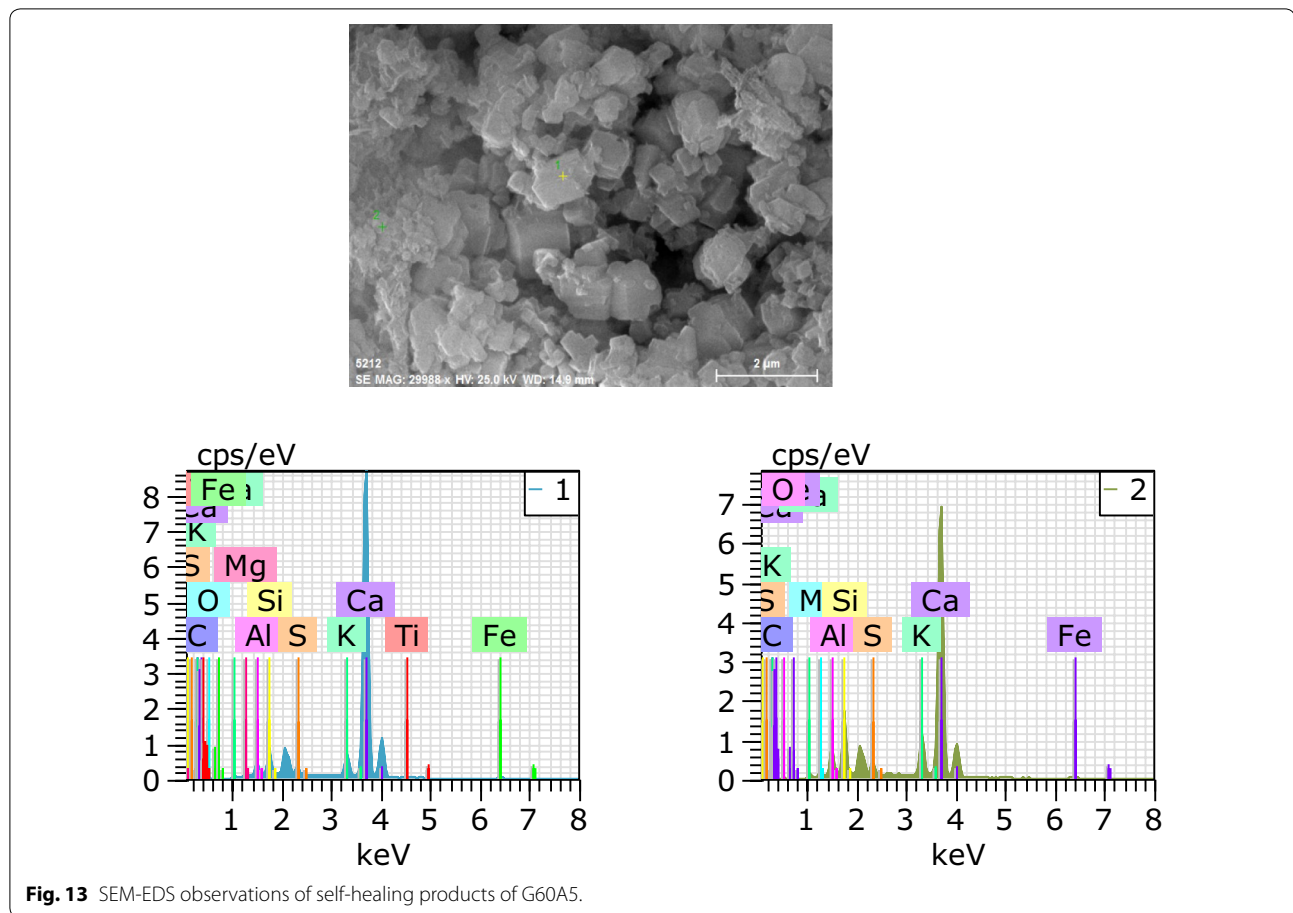
**d** G60A5



**e** C10X

**f** C10MX

**Fig. 12** SEM observations of self-healing products.



isothermal calorimetry, the water flow was significantly decreased in F35 and F50. This is because with FA, a reaction that generates stratlingite and ettringite needs the pH to be over a certain value; however, regarding isothermal calorimetry, the amount of mixing water was larger than that of the unreacted binders, which resulted in an inability to obtain a sufficient pH. Consequently, unreacted FA particles failed to react. In the case of the GGBFS and CA, the water flow continued to decrease because the unreacted GGBFS continued to react, and the hydrogarnet continued to react with the permeated  $\text{CO}_3^{2-}$  to produce  $\text{CaCO}_3$ . In the case of CSA-incorporated specimens, the water flow decreased rapidly. These results are the same as those of the isothermal calorimetry and are attributed to the ettringite produced by CSA.

In this study, the effect of self-healing products on self-healing concrete using inorganic binders was confirmed. The self-healing performance of CSA that can produce swelling hydrate was found to be the highest, and it was confirmed that the self-healing performance was improved even when GGBFS that can supply Al ions was incorporated. On the other hand, FA-based specimens

were found to be difficult in producing self-healing substances owing to further hydration unless they had a sufficient pH value.

#### Acknowledgements

This research was supported by a Grant (18SCIP-C120795-03) from Construction Technology Research Program funded by Ministry of Land, Infrastructure and Transport of Korean government. This research was also supported by a Grant (18SCIP-B103706-04) from Construction Technology Research Program funded by Ministry of Land, Infrastructure and Transport of Korean government.

#### Authors' contributions

All authors contributed substantially to all aspects of this article. Both authors read and approved the final manuscript.

#### Availability of data and materials

The data used to support the findings of this study are included within the article. In addition, some of the data used in this study is supported by the references mentioned in the article.

#### Competing interests

The authors declare that they have no competing interests.

#### Author details

<sup>1</sup> Construction Technology Research Center, Korea Conformity Laboratories, Seoul 08503, South Korea. <sup>2</sup> Department of Civil and Environmental Engineering, Gachon University, 1342 Seongnamdaero, Sujeong-gu, Seongnam-si, Gyeonggi-do 13120, Republic of Korea.

Received: 20 January 2019 Accepted: 14 May 2019  
Published online: 01 July 2019

## References

- Abdel-Jawad Y., & Dehn, F. (2005). Self-healing of self-compacting concrete. In proceedings of SCC, pp. 1023–1029, Chicago, USA.
- Ahn, T. H., & Kishi, T. (2010). Crack self-healing behavior of cementitious composites incorporating various mineral admixtures. *Journal of Advanced Concrete Technology*, 8, 171–186.
- Bouzoubaa, N., Zhang, M. H., Malhotra, V. M., & Golden, D. M. (1999). Blended fly ash cements—a review. *ACI Materials Journal*, 96, 641–650.
- Castellano, C. C., Bonavetti, V. L., Donza, H. A., & Irassar, E. F. (2016). The effect of w/b and temperature on the hydration and strength of blast furnace slag cements. *Construction and Building Materials*, 111, 679–688.
- Choi, S.-W., Bae, W.-H., Lee, K.-M., & Shin, K.-J. (2017). Correlation between crack width and water flow of cracked mortar specimens measured by constant water head permeability test. *Journal of the Korea Concrete Institute*, 29, 267–273.
- Darquennes, A., Olivier, K., Benboudjema, F., & Gagné, R. (2016). Self-healing at early-age, a way to improve the chloride resistance of blast-furnace slag cementitious materials. *Construction and Building Materials*, 113, 1017–1028.
- Day, R. L. (1992). The Effect of secondary ettringite formation on the durability of concrete: A literature analysis. PCA Research and Development Bulletin RD108T, Portland Cement Association.
- Edvardsen, C. (1999). Water permeability and autogenous healing of cracks in concrete. *ACI Materials Journal*, 96, 448–454.
- Ferreiro, S., Frías, M., de la Vigil Villa, R., & Sánchez de Rojas, M. I. (2013). The influence of thermal activation of art paper sludge on the technical properties of blended Portland cements. *Cement & Concrete Composites*, 37, 136–142.
- Gallucci, E., Mathur, P., & Scrivener, K. (2010). Microstructural development of early age hydration shells around cement grains. *Cement and Concrete Research*, 40, 4–13.
- Granger, S., Loukili, A., Pijaudier-Cabot, G., & Chanvillard, G. (2007). Experimental characterization of the self-healing of cracks in an ultra-high performance cementitious material: Mechanical tests and acoustic emission analysis. *Cement and Concrete Research*, 37, 519–527.
- Hearn, N. (1998). Self-sealing, autogenous healing and continued hydration: what is the difference? *Materials and Structures*, 31, 563–567.
- Hesse, C., Goetz-Neunhoeffler, F., & Neubauer, J. (2011). A new approach in quantitative in situ XRD of cement pastes: Correlation of heat flow curves with early hydration reactions. *Cement and Concrete Research*, 41, 123–128.
- Hewlett, P. C. (2004). *Lea's Chemistry of Cement and Concrete* (4th ed.). Amsterdam: Elsevier Science & Technology Books.
- Hilloulin, B., Hilloulin, D., Grondin, F., Loukili, A., & Belie, N. D. (2016). Mechanical regains due to self-healing in cementitious materials: Experimental measurements and micro-mechanical model. *Cement and Concrete Research*, 80, 21–32.
- Hu, X., Shi, C., Shi, Z., Tong, B., & Wang, D. (2017). Early age shrinkage and heat of hydration of cement-fly ash-slag ternary blends. *Construction and Building Materials*, 153, 857–865.
- Huang, H., Ye, G., & Damidot, D. (2013). Characterization and quantification of self-healing behaviors of microcracks due to further hydration in cement paste. *Cement and Concrete Research*, 52, 71–81.
- Huang, H., Ye, G., & Damidot, D. (2014). Effect of blast furnace slag on self-healing of microcracks in cementitious materials. *Cement and Concrete Research*, 60, 68–82.
- Jacobsen, S., Marchand, J., & Boisvert, L. (1996). Effect of cracking and healing on chloride transport in OPC concrete. *Cement and Concrete Research*, 26, 869–881.
- Jacobsen, S., & Sellevold, E. R. J. (1995). Self-healing of high strength concrete after deterioration by freeze/thaw. *Cement and Concrete Research*, 26, 55–62.
- Jaroenratanirom, D., & Sahamitmongkol, R. (2011). Self-crack closing ability of mortar with different additives. *Journal of Metals, Materials and Minerals*, 21, 9–17.
- Kim, T.-W., & Kang, C. (2017). The self-healing and aging effect of OPC-GGBFS cement in sea-water and tap-water. *Journal of the Korea Concrete Institute*, 29, 11–21.
- Le Saoût, G., & Haha, M. B. (2011). Effect of filler on early hydration, In *XIII International Congress on the Chemistry of Cement* Madrid, Spain.
- Lerch, W. (1946). The influence of gypsum on the hydration and properties of Portland cement pastes—discussion. *Proceedings-American Society for Testing and Materials*, 46, 1252–1297.
- Martin, L. H. J., Winnefeld, F., Tschopp, E., Müller, C. J., & Lothenbach, B. (2017). Influence of fly ash on the hydration of calcium sulfoaluminate cement. *Cement and Concrete Research*, 95, 152–163.
- Mota, B., Matschei, T., & Scrivener, K. (2018). Impact of NaOH and Na<sub>2</sub>SO<sub>4</sub> on the kinetics and microstructural development of white cement hydration. *Cement and Concrete Research*, 108, 172–185.
- Muhammad, N. Z., Shafaghat, A., Keyvanfar, A., Majid, M. Z. A., Ghoshal, S. K., Yasouj, S. E. M., et al. (2016). Tests and methods of evaluating the self-healing efficiency of concrete: A review. *Construction and Building Materials*, 112, 1123–1132.
- Nocun-Wczelik, W., Bochenek, A., & Migda, M. (2012). Calorimetry and other methods in the studies of expansive cement hydrating mixtures. *Journal of Thermal Analysis and Calorimetry*, 109, 529–535.
- Odler, I., & Dorr, H. (1979). Early hydration of tricalcium silicate II. *The induction period, Cement and Concrete Research*, 9, 277–284.
- Qiu, J., Tan, H. S., & Yang, E.-H. (2016). Coupled effects of crack width, slag content, and conditioning alkalinity on autogenous healing of engineered cementitious composites. *Cement & Concrete Composites*, 73, 203–212.
- Richardson, I. G., Wilding, C. R., & Dickson, M. J. (1989). The hydration of blast furnace slag cements. *Advances in Cement Research*, 2, 147–157.
- Roig-Flores, M., Moscato, S., Serna, P., & Ferrara, L. (2015). Self-healing capability of concrete with crystalline admixtures in different environments. *Construction and Building Materials*, 86, 1–11.
- Sahmaran, M., Yildirim, G., & Erdem, T. K. (2013). Self-healing capability of cementitious composites incorporating different supplementary cementitious materials. *Cement & Concrete Composites*, 35, 89–101.
- Salama, I., Hilloulin, B., Medjigbodo, S., & Loukili, A. (2017). Influence of supplementary cementitious materials on the autogenous self-healing of cracks in cementitious materials. *ACI special publication*, 320, 1–14.
- Shen, P., Lu, L., He, Y., Rao, M., Fu, Z., Wang, F., et al. (2018). Experimental investigation on the autogenous shrinkage of steam cured ultra-high performance concrete. *Construction and Building Materials*, 162, 512–522.
- Sherir, M. A. A., Hossain, K. M. A., & Lachemi, M. (2016). Self-healing and expansion characteristics of cementitious composites with high volume fly ash and MgO-type expansive agent. *Construction and Building Materials*, 30, 80–92.
- Sisomphon, K., Copuroglu, O., & Koenders, E. A. B. (2012). Self-healing of surface cracks in mortars with expansive additive and crystalline additive. *Cement & Concrete Composites*, 34, 566–574.
- Snoeck, D., & Belie, N. D. (2015). From straw in bricks to modern use of micro-fibers in cementitious composites for improved autogenous healing—A review. *Construction and Building Materials*, 95, 774–787.
- Snoeck, D., Malm, F., Cnudde, V., Grosse, C. U., & Tittelboom, K. V. (2018). Validation of self-healing properties of construction materials through non-destructive and minimal invasive Testing. *Advanced Materials Interfaces*, 5, 1800179.
- Termkhajornkit, P., Nawa, T., Yamashiro, Y., & Saito, T. (2009). Self-healing ability of fly ash-cement systems. *Cement & Concrete Composites*, 31, 195–203.
- Tittelboom, K. V., Gruyaert, E., Rahier, H., & Belie, N. D. (2012). Influence of mix composition on the extent of autogenous crack healing by continued hydration or calcium carbonate formation. *Construction and Building Materials*, 37, 349–359.
- Wua, M., Johannesson, B., & Geiker, M. (2012). A review: self-healing in cementitious materials and engineered cementitious composite as a self-healing material. *Construction and Building Materials*, 28, 571–583.

## Publisher's Note

Springer Nature remains neutral with regard to jurisdictional claims in published maps and institutional affiliations.